**Human
PATHOLOGY**

Original contribution

Pathological findings in the postmortem liver of patients with coronavirus disease 2019 (COVID-19)[☆,☆☆]

Chaohui Lisa Zhao MD, PhD [a,*], **Amy Rapkiewicz MD** [a],
Mona Maghsoodi-Deerwester MD [a], **Mala Gupta MD** [a], **Wenqing Cao MD** [b],
Thomas Palaia PhD [a], **Jianhong Zhou MD** [a], **Bebu Ram MD** [a], **Duc Vo MD** [a],
Behnam Rafiee MD [a], **Zarrin Hossein-Zadeh MD** [a], **Bahram Dabiri MD** [a],
Iman Hanna MD [a,**]

[a] *NYU Long Island School of Medicine, NYU Langone Hospital - Long Island, Department of Pathology, 11501, USA*
[b] *NYU Grossman School of Medicine, NYU Langone Health, Department of Pathology, 10016, USA*

Summary Although coronavirus disease 2019 (COVID-19) is transmitted via respiratory droplets, there are multiple gastrointestinal and hepatic manifestations of the disease, including abnormal liver-associated enzymes. However, there are not many published articles on the pathological findings in the liver of patients with COVID-19. We collected the clinical data from 17 autopsy cases of patients with COVID-19 including age, sex, Body mass index (BMI), liver function test (alanine aminotransaminase (ALT), aspartate aminotransaminase (AST), alkaline phosphatase (ALP), direct bilirubin, and total bilirubin), D-dimer, and anticoagulation treatment. We examined histopathologic findings in postmortem hepatic tissue, immunohistochemical (IHC) staining with antibody against COVID-19 spike protein, CD68 and CD61, and electron microscopy. We counted the number of megakaryocytes in liver sections from these COVID-19−positive cases. Abnormal liver-associated enzymes were observed in 12 of 17 cases of COVID-19 infection. With the exception of three cases that had not been tested for D-dimer, all 14 patients' D-dimer levels were increased, including the cases that received varied doses of anticoagulation treatment. Microscopically, the major findings were widespread platelet-fibrin microthrombi, steatosis, histiocytic hyperplasia in the portal tract, mild lobular inflammation, ischemic-type hepatic necrosis, and zone 3 hemorrhage. Rare megakaryocytes were found in sinusoids. COVID-19
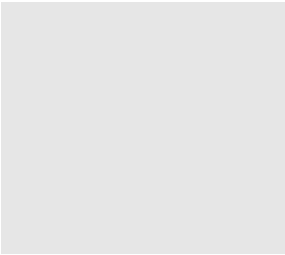

IHC demonstrates positive staining of the histiocytes in the portal tract. Under electron microscopy, histiocyte proliferation is present in the portal tract containing lipid droplets, lysosomes, dilated ribosomal endoplasmic reticulum, microvesicular bodies, and coronavirus. The characteristic findings in the liver of patients with COVID-19 include numerous amounts of platelet-fibrin microthrombi, as well as various degrees of steatosis and histiocytic hyperplasia in the portal tract. Possible mechanisms are also discussed.

1. Introduction

The coronavirus disease 2019 (COVID-19) pandemic is an ongoing global health emergency [1]. In symptomatic patients, the clinical manifestations of the disease usually present as fever, cough, fatigue, and loss of taste and smell. In severe cases, individuals exhibit symptoms of pneumonia, associated with complications of severe acute respiratory distress syndrome [1].

Although the virus is transmitted via respiratory droplets, there are multiple gastrointestinal and hepatic manifestations of the disease. Patients presented with gastrointestinal symptoms such as diarrhea, vomiting, and abdominal pain. Moreover, the abnormal liver-associated enzymes in patients who were infected were observed in a substantial proportion (from 16% to 60%) of patients, although generally only mildly elevated [2–5]. Some articles showed that more severe alterations in liver enzymes may correlate with worse symptoms of COVID-19 clinical courses [2].

The phenomenon of the liver involvement in COVID-19 infection may be related to the virus' use of angiotensin-converting enzyme 2 (ACE-2) receptors [2]. It is proven that ACE-2 cell surface receptors were expressed in liver cholangiocyte (59.7%) [6,7] higher than hepatocytes (2.6%) [3]. The level of ACE-2 in cholangiocytes was similar to that of type 2 alveolar cells of the lungs, indicating that the liver could be a potential target for COVID-19 [5]. Hypoxia and shock induced by COVID-19–related complications including respiratory distress syndrome, systemic inflammatory response syndrome, and multiple organ failure could be other reasons that cause liver damage. Importantly, the presence of megakaryocytes in various organs in COVID-19–positive patients and a prominent feature of macrovascular and microvascular thrombosis reported by Rapkiewicz [8] are interesting findings, which may also contribute to the injury of the liver.

However, there are not many publications concerning the pathological findings in the liver of COVID-19–positive patients. In this article, we collected the data from 17 autopsy cases of patients with COVID-19 to demonstrate the histopathological characteristics.

2. Materials and methods

The study was performed in accordance with the ethical guidelines and approval from the institutional review board of New York University Langone Medical Center, New York, NY 10016.

2.1. Patients and data collection

Hospital-based autopsies were performed by the director of autopsy service using personal protective equipment in a negative pressure facility with limited staff participation to reduce risk [8]. Consecutive autopsies performed at NYU Langone Hospital, Long Island, among persons with laboratory-confirmed COVID-19 or who were under investigation and tested positive on postmortem polymerase chain reaction (PCR) were included [8]. Hepatic tissue was fixed in 10% buffered formalin for 72 h and then routinely processed.

Chart review was performed to identify medical history, laboratory values (initial and peak, when available), and treatment including anticoagulation, antibiotics, and experimental antiviral drugs.

2.2. Histopathology assessment

To assess hepatic morphology, sections were stained with hematoxylin and eosin and Masson's trichrome. Histological assessment and scoring were performed by three pathologists blinded to the study. Steatosis was graded as follows: grade 0: <5%, grade 1: 5–33%, grade 2: 34–66%, and grade 3: >66% [9].

2.3. Immunohistochemical staining

Paraffin-embedded tissues were cut to 4-μm sections, deparaffinized, and rehydrated with xylene and graded alcohols. Immunohistochemical (IHC) staining was performed on a Ventana BenchMark Ultra (Roche, MI, USA) using Optiview DAB IHC detection kit (Ventana Medical Systems, Tucson, AZ). Antigen retrieval was performed in 95 C for 64 min. Mouse monoclonal

antibody of COVID-19 spike protein (clone1A9; GTX632604; GeneTex, CA, USA) was used in 1:800 dilution. CD68 primary antibody (clone number: KP-1) was obtained from Ventana Medical Systems (Tucson, AZ). cytomegalovirus (CMV) primary mouse monoclonal antibody (clone number 8B1.2, 1G5.2 & 2D4.2) was obtained from Cell Marque (Rocklin, CA). Slides were counterstained with hematoxylin.

2.4. Numbers of megakaryocytes

We counted the number of megakaryocytes in the livers of 13 COVID-19 cases and, for comparison, 13 cases of patients who died due to other causes, selected from autopsies previously performed at NYU Winthrop Hospital between 2017 and 2019. Ten consecutive high-power fields (HPF, 40x magnification) were scored three times for each case.

2.5. Electron microscopy

For electron microscopy, tissue samples were fixed in 4% glutaraldehyde buffered in 0·1 M sodium cacodylate buffer, pH 7.5, washed in sodium cacodylate buffer, post-fixed in buffered 1% osmium tetroxide with 0.5% potassium ferricyanide, en bloc stained with a saturated solution of uranyl acetate in 40% ethanol, dehydrated in a graded series of ethanol, infiltrated in propylene oxide with Epon epoxy resin (LX112, Ladd industries, Burlington, VT), and embedded. Blocks were sectioned with a Reichert Ultracut microtome at 70 nm. The resulting grids were poststained with 1% aqueous uranyl acetate followed by 0·5% aqueous lead citrate and scoped on a Zeiss EM 900 transmission electron microscope retrofitted with an L3C digital camera (SIA, Duluth, GA).

2.6. Epstein-Barr virus (EBV) in situ hybridization

The tests of EBV in situ hybridization were performed at Integrated Oncology LabCorp Specialty Testing Group (www. Integratedoncology.com) and interpreted by C.L.Z. with adequate controls provided.

2.7. Statistical analysis

Student's t-test was used to compare the number of megakaryocytes between COVID-19 and non-COVID-19 cases. P values < 0·05 were considered statistically significant.

3. Results

The clinical presentation of the 17 cases is summarized in Table 1 for the patient's age, sex, BMI, past medical history, viral serologies, peak alanine aminotransaminase (ALT), peak aspartate aminotransaminase (AST), peak alkaline phosphatase (ALP), total bilirubin, direct bilirubin, liver weight, peak D-dimer, anticoagulation treatmen,t and the level of the last D-dimer. Other relevant information was summarized in Supplemental Table 1, including the COVID-19 test result, reason for admission, respiratory symptoms and other symptoms, other relevant treatments (receiving respiratory assistance and nonanticoagulation), days of symptom onset to death, days of hospitalization to death, and days of receiving invasive mechanical ventilation to death.

3.1. Age

There were 10 men (58.8%) and 7 women (41.2%). The age range for these 17 cases was 44−85 years with an average age of 65.24 years. The deceased women aged 50−85 years with an average age of 67 years. The deceased men aged 44−83 years with an average age of 64 years.

3.2. Body mass index (BMI)

The BMI of these autopsy cases was higher than normal with a range of 23−52 kg/m^2 and a mean of 31.7 kg/m^2. The BMI of female cases was 32.83 kg/m^2, and the BMI of male cases was 30.95 kg/m^2.

3.3. Liver function test

Abnormal liver-associated enzymes were observed in 12 of 17 cases. AST was increased in 12 cases including 4 cases which were significantly increased (>3500 IU/L). ALT was increased in 11 cases including 5 cases which were significantly increased (>1200 IU/L). ALP was increased in 6 cases. However, only mild increase of bilirubin was appreciated (8 cases for direct bilirubin and 2 cases for total bilirubin).

3.4. D-dimer and anticoagulation treatment

With the exception of three cases (case 1, 2, 3) that had not been tested for D-dimer, all 14 patients' d-dimer levels were increased (normal: <309 ng/ml). The patients tested for D-dimer had received varied doses of anticoagulation treatment (Table 1) except for case 13 which had a large acute territorial infarction and as such tissue plasminogen activator was not given due to aortic dissection.

3.5. Pathological findings

Microscopically, there were eight major findings in the 17 autopsy cases, which are separated into two groups including features of COVID-19 infection and secondary changes or other causes (Table 2).

Table 1 Clinical information.

Case number	Age	Sex	BMI kg/m²	Medical history	Viral serologies	Peak ALT (IU/L)	Peak AST (IU/L)	Peak ALP (IU/L)	Total bilirubin (mg/dl)	Direct bilirubin (mg/dl)	Liver weight (gram)	Peak D-dimer (ng/ml)	Anticoagulation treatment	Last D-dimer (ng/ml)
Case 1	64	F	36.1	COPD, lung cancer, HTN, HLP	HCV-	39	30	84	0.2	N/A	2585	N/A	No	N/A
Case 2	60	M	32.3	CAD, HTN	N/A	36	48	54	0.5	0.2	1760	N/A	No	N/A
Case 3	50	F	23	HTN, HLP	HBV-, HCV-	4545	>3500	200	0.9	0.7	1670	N/A	Enoxaparin 40 mg daily	N/A
Case 4	44	M	38.8	Renal cell carcinoma, HTN, HLP	HBV-, HCV-	146	58	57	0.5	0.3	1570	320	Unfractionated heparin drip	320
Case 5	66	F	34.4	Obstructive sleep apnea, HTN, HLP	HBV-, HCV-	2025	5508	92	0.9	0.5	1890	10,287	Aspirin and unfractionated heparin drip, then transitioned to enoxaparin 1 mg/kg q12h	10,287
Case 6	56	F	30.5	No significant PMH	HBV-, HCV-	84	93	210	1.7	1.4	1795	5483	Enoxaparin 40 mg daily, transitioned to unfractionated heparin drip, then enoxaparin 1 mg/kg q12h	699
Case 7	65	M	25.01	Cirrhosis, CKD, HTN	HBV-, HCV-	60	87	83	2	1.2	1650	>52,926	Unfractionated heparin drip	>52,926
Case 8	71	F	33.2	CAD, DM II, HTN, HLD	N/A	19	28	68	0.4	0.1	1500	2112	Enoxaparin 90 mg daily	1048
Case 9	60	M	52	CAD, CHF, HTN	N/A	1295	272	91	1.6	0.5	2600	4532	Apixaban 5 mg q12h	509
Case 10	85	F	29.8	Asthma	N/A	40	63	176	1	0.7	1000	804	Unfractionated heparin 5000 units subcutaneous tid	804
Case 11	77	F	42.8	CAD, DM II	HAV-, HBV-, HCV-	25	32	110	1.1	0.9	1300	7095	Unfractionated heparin 5000 units subcutaneous tid, transitioned to heparin drip	4646
Case 12	83	M	23.2	CHF, HTN, DVT	N/A	13	33	76	1.1	0.7	1460	51,336	Unfractionated heparin drip	8875
Case 13	58	M	31	CVA with type A aortic dissection, HTN, acute	HBV-, HCV-	21	24	89	0.3	0.2	2160	11,272	No	10,510

Case	Age	Sex	BMI		PMH	Hepatitis								Anticoagulation	
Case 14	71	M	26.69	territorial infarction	CAD, DM II, HTN	HAV-, HBV-, HCV-	73	40	118	0.2	0.1	1780	2000	Enoxaparin 40 mg daily	210
Case 15	72	M	29.14		CAD, HTN, HLP, DM II, CKD	HBV-, HCV-	25	40	66	0.3	0.2	2070	6668	Unfractionated heparin drip	2035
Case 16	58	M	27.4		No significant PMH	N/A	6136	13,592	183	2	1.9	2190	>52,926	Unfractionated heparin drip	>52,926
Case 17	69	M	24		DM II, Parkinson disease, seizure	N/A	3422	8913	98	0.7	0.6	1100	10,950	Enoxaparin 40 mg daily	7850

CAD, coronary artery disease; CHF, congestive heart failure; CKD, chronic kidney failure; COPD, Chronic obstructive pulmonary disease; CVA, cerebrovascular accident; DM II, type II diabetes; HAV-, negative for hepatitis A; HBV-, negative for hepatitis B; HCV-, negative for hepatitis C; HLP, hyperlipidemia; HTN, hypertension; PMH, past medical history; DVT, deep vein thrombosis.

3.5.1. Platelet-fibrin microthrombi

Platelet-fibrin microthrombi were present in the sinusoid, central vein, or portal vein (Fig. 1A−B) in 12 of the 17 cases (case 1, 2, 3, 4, 5, 6, 7, 8, 12, 13, 14, 17). One case (case 5) demonstrated red blood cells with abnormal morphology (burr cells or schistocytes; Fig. 1C) beside microthrombi. However, the patient did not have a history of sickle cell disease. IHC staining for CD61 (platelet glycoprotein IIIa, a megakaryocytic and platelet marker) highlighted platelet microthrombi in the sinusoid, central vein, or portal vein (Fig. 1D).

3.5.2. Numbers of megakaryocytes

Megakaryocytes were seen in some cases (case 2, 3, 5, 6, 8, 10, 11, 13, 14, 15, 16; Fig. 1E). The mean number of megakaryocytes/10 HPF in the liver was 1.08 ± 0.15 in patients with COVID-19. It was higher than the number of megakaryocytes in the control cases ($p < 0.01$), which is $0 \pm 0/10$ HPF.

3.5.3. Histiocytic hyperplasia

Five cases (case 1, 5, 6, 12, 15) demonstrated significantly increased number of histiocytes with vacuolated cytoplasm in the portal tract (Fig. 2A). CD68 stain confirmed histiocytic hyperplasia (Fig. 2B). These vacuolated histiocytes were positive for the COVID-19 IHC stain (Fig. 2C).

3.5.4. Steatosis

Steatosis (Fig. 1A and F) was appreciated in 12 of 17 cases (case 1, 2, 3, 4, 5, 7, 8, 9, 10, 11, 12, 16) with 4 cases grade 2 and 8 cases grade 1 steatosis. The majority of cases (7 of 12 cases) showed a predominant macrovesicular pattern, while 4 cases were mixed macrovesicular/microvesicular pattern, and only one case was predominantly microvesicular pattern.

3.5.5. Lobular inflammation

Lobular inflammation was present in 5 of 17 cases (case 1, 2, 3, 5, 14) with mild sinusoidal infiltrate of lymphocytes (Supplemental Fig. 1A). The lymphocytes were arranged in a single file. This lobular predominant inflammation was associated with hepatocyte injury, with scattered acidophil bodies (Supplemental Fig. 1B).

3.5.6. Portal tract inflammation

In the portal tract, mild lymphocyte and plasma cell infiltrates were noted in 8 of 17 cases (case 1, 4, 5, 6, 10, 11, 12, 13; Supplemental Fig. 1C). No significant interface activity was identified in these cases. The portal tracts were essentially normal in the other 9 cases.

Table 2 Microscopy findings in the postmortem liver.

| Histological findings	Number of the case (%)
Features of COVID-19 infection	
Platelet-fibrin thrombi in the sinusoid, central vein, or portal vein	12/17 (70.6%)
Rare megakaryocytes found in sinusoids	11/13 (84.6%)
Histiocytic hyperplasia	5/17 (29.4%)
Secondary changes or other causes	
Steatosis	12/17 (70.6%)
Lobular inflammation	5/17 (29.4%)
Portal tract inflammation (mild)	8/17 (47%)
Ischemic-type hepatic necrosis	2/17 (11.8%)
Zone 3 hemorrhage/necrosis	8/17 (47%)

3.5.7. Ischemic-type hepatic necrosis and zone 3 hemorrhage

Zone 3 hemorrhage and necrosis was noted in 8 of 17 cases (case 1, 3, 5, 6, 9, 13, 15, 16). Ischemic-type hepatic necrosis was noted in 2 of 17 cases (case 3, 6).

3.6. COVID-19 stain

COVID-19 IHC demonstrated positive staining in the histiocytes in the portal tracts (Fig. 2C and D) in 5 of 17 cases (29.4%) with weak to moderate staining. In addition, days to symptom onset to death of all 5 cases were less than two weeks. Cholangiocytes also had weak staining (Fig. 2C). In contrast, endothelial cells of the portal vein were negative for COVID-19 IHC stain. Hepatocytes presented nonspecific IHC stain, compared with negative tissue control. To rule out nonspecific stains, pictures of H&E stain demonstrate that there was no pigmentation identified in the portal tracts including histiocytes and cholangiocytes (Supplemental picture 2A and B). Negative controls for IHC COVID-19 stains also revealed that hepatocytes presented nonspecific weak IHC stain but no nonspecific stains presented in the portal tracts (Supplemental picture 2C).
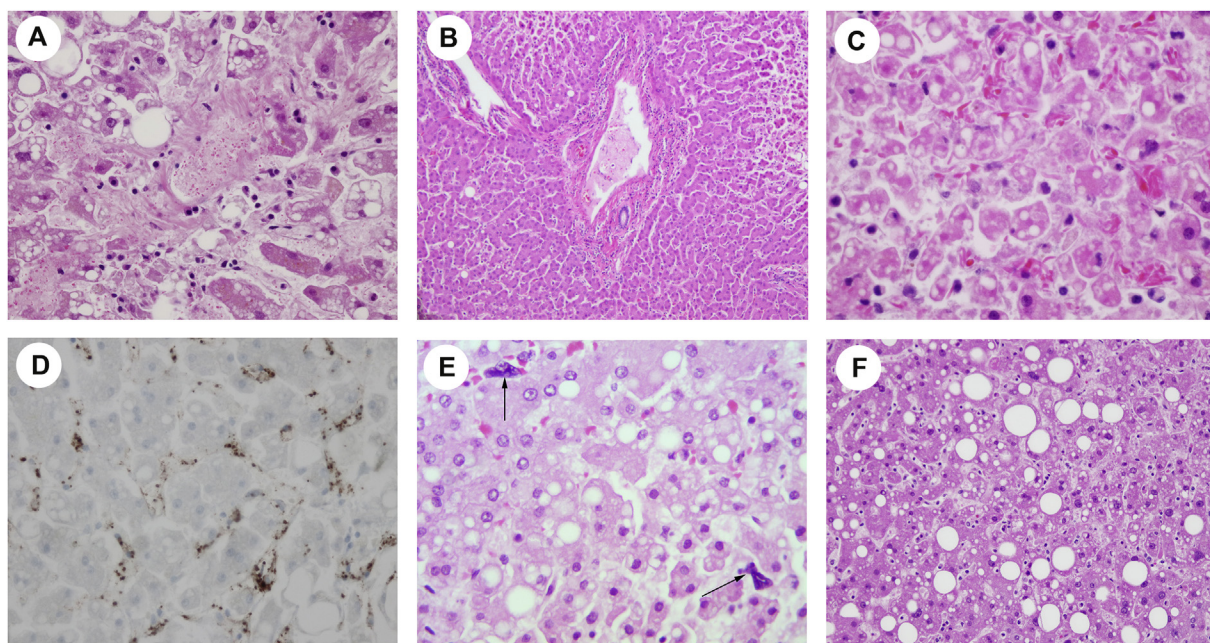
Fig. 1 (A) Platelet-fibrin thrombi are present in the sinusoidal spaces and central vein (H&E, ×400). Macrovesicular and microvesicular steatoses are also demonstrated. (B) Platelet-fibrin thrombus is present in the portal vein (H&E, ×200). (C) Burr cells are appreciated in the sinusoid with macrovesicular and microvesicular steatosis in adjacent hepatic cells (H&E, ×400). (D) Platelet-fibrin microthrombi in the sinusoid are positive for CD61 IHC stain (×400). (E) Megakaryocytes (arrows) were seen in the sinusoid (×400). (F) Steatosis (H&E, ×100).
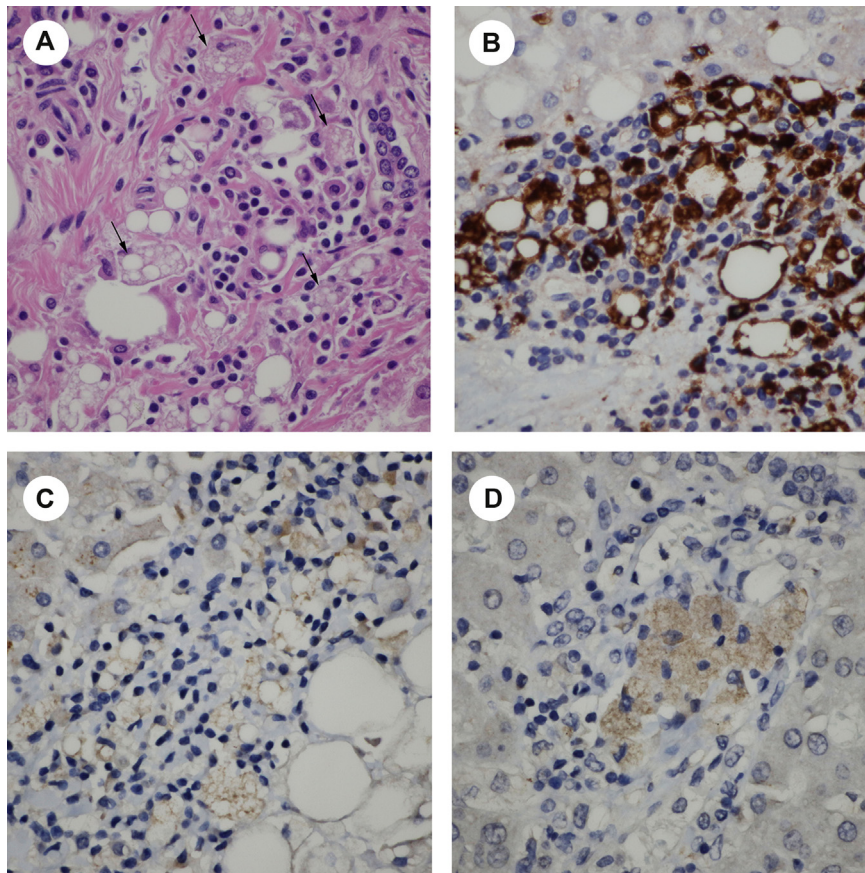
Fig. 2 Histiocytic hyperplasia in the portal tract. (A) There is significant histiocytic proliferation in the portal tract with vacuolated changes in the cytoplasm of histiocytes (black arrow; H&E, ×600). (B) CD68 stain confirms histiocytic hyperplasia (×600). (C) and (D): These vacuolated histiocytes are positive for COVID-19 IHC stain (×600).
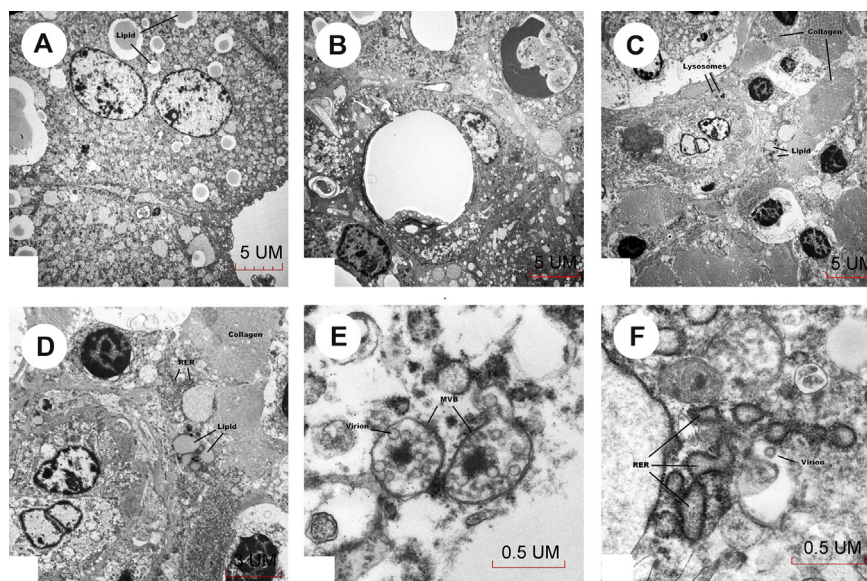
3.7. Electron microscopy

Survey showed hepatocytes containing lipid droplets (Fig. 3A). Histiocytic proliferation was present in portal tracts around bile ducts (Fig. 3B) and in areas of collagenous connective tissue. Histiocytes contained lipid droplets, lysosomes (Fig. 3C), dilated rough endoplasmic reticulum (RER; Fig. 3D), and microvesicular bodies (Fig. 3E). A virion-like particle was seen in Fig. 3F at approximately 80 nm in size near dilated RER, and microvesicular bodies containing similar size virus particles were seen in Fig. 3E, which were consistent with the morphology of severe acute respiratory syndrome (SARS) coronavirus [10].

4. Discussion

In these 17 autopsy cases, we demonstrated the pathological findings including numerous amounts of platelet-fibrin microthrombi in the hepatic sinusoids, central vein, or portal vein and rare megakaryocytes found in sinusoids. These findings were consistent with the previously published findings of one of our authors, Rapkiewicz [8]. She reported platelets in widespread microvascular thrombosis in multiple organs of patients with COVID-19. In addition,

she also noted megakaryocytes in the microvasculature of the heart, in glomeruli, and in increased numbers in the lungs and bone marrow in COVID-19 autopsies [8]. These support that the phenomenon of platelet microthrombi and megakaryocytes in the microvasculature in the liver might be associated with the systemic damage of COVID-19.

Several articles have described the hepatic involvement in COVID-19. Xu et al. [11] demonstrated the presence of moderate microvesicular steatosis and mild inflammatory infiltrates in the hepatic lobule and portal tract in the first postmortem findings of a patient with COVID-19 . Tian et al. [12] reported mild sinusoidal dilatation, focal macrovesicular steatosis, and mild lobular lymphocytic infiltration in four patients with COVID-19. No significant bile duct damage was identified [12]. Lagana et al. [13] also reported macrovesicular steatosis, mild lobular necroinflammation, and portal inflammation. Our report presents similar findings including steatosis, lobular inflammation, and mild portal tract inflammation. Bile duct injury was also not observed in our study. Moreover, we present the unique findings including widespread platelet-fibrin microthrombi, histiocytic hyperplasia in the portal tracts, and rare megakaryocytes found in sinusoids.

Fig. 3 Electron microscopy. (A) Hepatocytes contain lipid droplets. (B) Histiocytes contain lipid droplets. (C) Histiocytes contain lysosomes. (D) Histiocytes contain dilated RER. (E) Microvesicular bodies contain COVID-19 virus. (F) COVID-19 virus is approximately 80 nm in size and identified near dilated rough endoplasmic reticulum (ER).

In our autopsy cases, platelet-fibrin microthrombi were found in 12 of the 17 cases (70%). However, vascular pathology including sinusoidal microthrombi was infrequent, seen in only 15% cases in Lagana's group [13]. The difference may be caused by whether or not the patients received anticoagulation treatment and the level of D-dimer just before the patient passed away. Adequate anticoagulation treatment may dramatically change the findings of sinusoidal microthrombi in the postmortem liver.

One post postmortem liver (case 7) showed cirrhosis because the patient had a history of alcoholic cirrhosis (Table 1), which was not related to the COVID-19 infection.

Although we had 17 cases, the numbers of megakaryocytes were only counted in 13 cases because of the variable levels of autolysis in the remaining four cases.

Platelets have been shown to play an important role in regulating intravascular inflammation through the huge array of soluble mediators and cell surface molecules expressed by platelets [14]. It is clear that platelets can not only activate and recruit leukocytes to the sites of infection and inflammation but also modulate leukocyte behavior with enhancing their ability to phagocytose and induce the production of neutrophil extracellular traps (NETs) [14]. NETs can directly damage epithelial and endothelial cells and are also linked to hepatic damage [15]. Together with ischemic-type hepatic necrosis associated with the microthrombi, these observations suggest that profound platelet-fibrin microthrombi in COVID-19 may be responsible in part for liver damage. It not only provides a window into the fatal mechanisms of COVID-19 disease [8] but also explains the clinical findings of abnormal liver function tests and high D-dimer in patients with COVID-1 9.

We observed histiocytic hyperplasia in the portal tract in these COVID-19 autopsies. Histiocytic hyperplasia was also identified in the lungs of patients with COVID-19 [16]. During infection, histiocytes/macrophages play an important role in immune defense and immune pathogenesis by frequently interacting with the ACE-2−expressing cells [6]. Macrophages may be recruited by ACE-2−expressing cells including cholangiocytes through CD74-MIF interaction and other signaling pathways. CD74 is a nonpolymorphic type II transmembrane glycoprotein, which was expressed on the cell surface of antigen-presenting cells including histiocytes/macrophages [17]. In addition, it is clear that CD74 also regulates trafficking of angiotensin II type I receptor (AT1) [17]. CD74 directly impedes AT1 intracellular trafficking and consequently causes AT1 accumulation in the endoplasmic reticulum (ER) and promotes AT1 proteasomal degradation [18]. MIF is the macrophage migration inhibitory factor, which plays a role in inflammatory and immune responses as a proinflammatory cytokine [6]. This may be a possible mechanism for histiocytic hyperplasia in the portal tract and also explains the reason why the viral copy number was so high that it was also detectable by IHC staining of COVID-19 spike protein and detecting COVID-19 in the ER of histiocytes under the electron microscope. In summary, the COVID-19 infection leads to macrophage activation and secondary inflammatory reactions [19]. Subsequently, inflammatory reactions attack the infected cells, leading to apoptosis and necrosis.

Although ACE-2 receptors were seen in the hepatocytes and cholangiocytes [20,21], our results showed only

histiocytes in the portal tract and that cholangiocytes demonstrated positive IHC COVID-19 stain in some cases. Endothelial cells of the portal vein were negative for the COVID-19 IHC stain. Hepatocytes showed only nonspecific IHC staining. However, an article from Ackermann [22] et al. showed that lungs from patients with COVID-19 demonstrated severe endothelial injury associated with the presence of intracellular virus and disrupted cell membranes. Therefore, the negative COVID-19 IHC stain did not entirely rule out the infection in endothelial cells and hepatocytes because IHC staining is not a sensitive method for detecting viruses compared with other detection methods such as PCR.

Abnormal liver-associated enzymes were observed in most of our autopsy cases. Moreover, some cases presented significantly increased liver-associated enzymes. In addition, microscopically, lobular inflammation with scattered acidophil bodies was present. Lymphocytes were arranged in a single file in the sinusoids. The portal tracts demonstrated mild lymphocytic infiltrate without significant interface hepatitis. Mild lobular and portal inflammation on liver histology was also appreciated in other autopsy articles [8,11]. All of these may demonstrate a pattern with nonhepatotropic viral hepatitis. For example, EBV hepatitis is characterized by a similar pattern, which shows diffuse sinusoidal infiltrate typically composed of small lymphocytes arranged in a single-file *string-of-beads* pattern [23]. To rule out the possibilities of other viral infections, EBV in situ hybridization and CMV IHC staining were performed on the cases with nonhepatotropic viral hepatitis pattern (5 cases). All of these cases were negative for EBV and CMV infections (Supplemental Fig. 3). In addition, there was no serologic evidence of hepatitis A, hepatitis B, and hepatitis C infection.

Only 5 cases showed COVID-19 IHC positive staining. In addition, days to symptom onset to death of all 5 cases were less than two weeks. Other articles only used PCR to prove that the virus invaded the liver. For example, PCR of the liver tissue was positive in 11 of 20 patients tested (55%) in the study by Lagana et al [13]. The IHC stains and electron microscopy tests are not as sensitive as PCR. However, this is the first article to prove that the COVID-19 virus was present in the histiocytes and cholangiocytes of the liver via IHC and electron microscopy.

Although COVID-19 may contribute to liver dysfunction directly by an inflammatory response, all of the aforementioned findings suggest that COVID-19−related liver dysfunction may be mainly caused by secondary liver damage by respiratory distress syndrome-induced hypoxia, multiple organ failure, and the use of potentially hepatotoxic drugs [5,24]. However, it is difficult to separate the independent effect of viral infection from various treatment modalities, including antibiotics and experimental antiviral drugs that were used in these patients.

Steatosis is a common finding in these COVID-19 autopsies. There may be two reasons for steatosis. One is that the patients have a high BMI. Another is that it may be due to hypoxia and shock induced by COVID-19−related complications including respiratory distress syndrome, systemic inflammatory response syndrome, and multiple organ failure. All of these conditions may also cause hepatic ischemia and hypoxia-reperfusion dysfunction. It is well documented that shock and hypoxic conditions could lead to lipid accumulation in hepatocytes and then cause liver damage [5,24−26]. Other autopsy studies showed microvesicular steatosis in patients with COVID-19 [8,11,13]. Zone 3 hemorrhage could be nonspecific abnormalities related to infection, sepsis, or hypoxia.

5. Conclusion

In summary, we found numerous amounts of platelet-fibrin microthrombi in the hepatic sinusoids, central vein, or portal vein in livers of patients with COVID-19, as well as mixed macrovesicular and microvesicular steatosis, histiocytic hyperplasia, mild inflammatory infiltrate, and ischemic-type hepatic necrosis along with zone 3 hemorrhage.

Ethical approval

Reporting of this series of clinically indicated autopsies was exempted by the NYU Grossman School of Medicine Institutional Review Board. Consent was provided by the legal next of kin in each case.

Appendix A. Supplementary data

Supplementary data to this article can be found online at https://doi.org/10.1016/j.humpath.2020.11.015.

References

[1] Chen N, et al. Epidemiological and clinical characteristics of 99 cases of 2019 novel coronavirus pneumonia in Wuhan, China: a descriptive study. Lancet 2020;395:507−13.

[2] Agarwal A, et al. Gastrointestinal and liver manifestations of COVID-19. J Clin Exp Hepatol 2020;10:263−5.

[3] Cheong J, et al. Gastrointestinal and liver manifestations of COVID-19. Saudi J Gastroenterol 2020.

[4] Huang C, et al. Clinical features of patients infected with 2019 novel coronavirus in Wuhan, China. Lancet 2020;395:497−506.

[5] Jothimani D, et al. COVID-19 and liver. J Hepatol 2020.

[6] Qi F, et al. Single cell RNA sequencing of 13 human tissues identify cell types and receptors of human coronaviruses. Biochem Biophys Res Commun 2020;526:135−40.

[7] Zou X, et al. Single-cell RNA-seq data analysis on the receptor ACE2 expression reveals the potential risk of different human organs vulnerable to 2019-nCoV infection. Front Med 2020;14:185−92.

[8] Rapkiewicz AV, et al. Megakaryocytes and platelet-fibrin thrombi characterize multi-organ thrombosis at autopsy in COVID-19: a case series. EClinicalMedicine 2020;24. 100434-100434.

[9] Levene AP, et al. Quantifying hepatic steatosis - more than meets the eye. Histopathology 2012;60:971−81.

[10] Goldsmith CS, et al. Ultrastructural characterization of SARS coronavirus. Emerg Infect Dis 2004;10:320−6.

[11] Xu Z, et al. Pathological findings of COVID-19 associated with acute respiratory distress syndrome. Lancet Respir Med 2020;8:420−2.

[12] Tian S, et al. Pathological study of the 2019 novel coronavirus disease (COVID-19) through postmortem core biopsies. Mod Pathol 2020;33:1007−14.

[13] Lagana SM, et al. Hepatic pathology in patients dying of COVID-19: a series of 40 cases including clinical, histologic, and virologic data. Mod Pathol 2020;33:2147−55.

[14] Jenne CN, Kubes P. Platelets in inflammation and infection. Platelets 2015;26:286−92.

[15] Papayannopoulos V. Neutrophil extracellular traps in immunity and disease. Nat Rev Immunol 2018;18:134−47.

[16] Prieto-Perez L, et al. Histiocytic hyperplasia with hemophagocytosis and acute alveolar damage in COVID-19 infection. Mod Pathol 2020.

[17] Su H, et al. The biological function and significance of CD74 in immune diseases. Inflamm Res 2017;66:209−16.

[18] Szaszak M, et al. Identification of the invariant chain (CD74) as an angiotensin AGTR1-interacting protein. J Endocrinol 2008;199:165−76.

[19] Prompetchara E, Ketloy C, Palaga T. Immune responses in COVID-19 and potential vaccines: lessons learned from SARS and MERS epidemic. Asian Pac J Allergy Immunol 2020;38:1−9.

[20] Pan L, et al. Clinical characteristics of COVID-19 patients with digestive symptoms in hubei, China: a descriptive, cross-sectional, multicenter study. Am J Gastroenterol 2020;115:766−73.

[21] Chai X, et al. Specific ACE2 expression in cholangiocytes may cause liver damage after 2019-nCoV infection. 2020. p. 2020. 02.03.931766.

[22] Ackermann M, et al. Pulmonary vascular endothelialitis, thrombosis, and angiogenesis in covid-19. N Engl J Med 2020;383:120−8.

[23] Schechter S, Lamps L. Epstein-barr virus hepatitis: a review of clinicopathologic features and differential diagnosis. Arch Pathol Lab Med 2018;142:1191−5.

[24] Feng G, et al. COVID-19 and liver dysfunction: current insights and emergent therapeutic strategies. J Clin Transl Hepatol 2020;8:18−24.

[25] Zhang XJ, et al. An ALOX12-12-HETE-GPR31 signaling axis is a key mediator of hepatic ischemia-reperfusion injury. Nat Med 2018; 24:73−83.

[26] Chen J, et al. Hypoxia exacerbates nonalcoholic fatty liver disease via the HIF-2alpha/PPARalpha pathway. Am J Physiol Endocrinol Metab 2019;317:E710−22.